^{13}C-^{13}C rotational resonance in a transmembrane peptide: A comparison of the fluid and gel phases

Denis B. Langlais,[1] Robert S. Hodges,[2] and James H. Davis[3,*]
[1]*Department of Physics, Simon Fraser University, Burnaby, British Columbia, Canada V5A 1S6*
[2]*Department of Biochemistry, University of Alberta, Edmonton, Alberta, Canada T6G 2E8*
[3]*Department of Physics, University of Guelph, Guelph, Ontario, Canada N1G 2W1*
(Received 13 May 1998)

A comparative study of two doubly ^{13}C labeled amphiphilic transmembrane peptides was undertaken to determine the potential of rotational resonance for measuring internuclear distances through the direct dipolar coupling in the presence of motion. The two peptides, having the sequence acetyl-K_2-G-L_{16}-K_2-A-amide, differed only in the position of ^{13}C labels. The first peptide, $[1\text{-}^{13}C]leu_{11}:[\alpha\text{-}^{13}C]leu_{12}$, had labels on adjacent residues, at the carbonyl of leu_{11} and the α carbon of leu_{12}. The second, $[1\text{-}^{13}C]leu_8:[\alpha\text{-}^{13}|C]leu_{11}$, was labeled on consecutive turns of the α-helical peptide. The internuclear distance between labeled positions of the first peptide, which for an ideal α helix has a value of 2.48 Å, is relatively independent of internal flexibility or peptide conformational change. The dipolar coupling between these two nuclei is sensitive to motional averaging by molecular reorientation, however, making this peptide ideal for investigating these motions. The internuclear distance between labels on the second peptide has an expected static ideal α-helix value of 4.6 Å, but this is sensitive to internal flexibility. In addition, the dipolar coupling between these two nuclei is much weaker because of their larger separation, making this peptide a much more difficult test of the rotational resonance technique. The dipolar couplings between the labeled nuclei of these two peptides were measured by rotational resonance in the dry peptide powders and in multilamellar dispersions with dimyristoylphosphatidylcholine in the gel phase, at $-10\,°C$, and in the fluid phase, at $40\,°C$. The results for the peptide having adjacent labels can be readily interpreted in terms of a simple model for the peptide motion. The results for the second peptide show that, in the fluid phase, the motionally averaged dipolar coupling is too small to be measured by rotational resonance. Rotational resonance, rotational echo double resonance, and related techniques can be used to obtain reliable and valuable dipolar couplings in static solid and membrane systems. The interpretation of these couplings in terms of internuclear distances is straightforward in the absence of molecular motion. These techniques hold considerable promise for membrane protein structural studies under conditions, such as at low temperatures, where molecular motion does not modulate the dipolar couplings. However, a typical membrane at physiological temperatures exhibits complex molecular motions. In the absence of an accurate and detailed description of both internal and whole body molecular motions, it is unlikely that techniques of this type, which are based on extracting distances from direct internuclear dipolar couplings, can be used to study molecular structure under these conditions. Furthermore, the reduction in the strengths of the dipolar couplings by these motions dramatically reduces the useful range of distances which can be measured. [S1063-651X(99)08005-8]

PACS number(s): 87.15.By, 87.16.Dg

Accurately determining structural detail at a molecular level in systems exhibiting little long-range order, strong short-range order, and highly anisotropic molecular motions is an important but difficult challenge. In addition, in a biological membrane the molecules of interest are large (10's or 100's of kD) and are only a minor component of a complex heterogeneous mixture. The determination of membrane protein structure, even on a local scale, and of the conformational changes which occur under physiological conditions is of tremendous interest and importance to researchers in all fields of medicine and biology. Fortunately, many of the techniques required to solve this sort of problem already exist.

Solution state nuclear magnetic resonance (NMR) takes advantage of rapid isotropic motional averaging, through the reorientation of individual molecules or of molecular aggregates such as micelles, which removes the strong orientation-dependent tensor interactions which would otherwise broaden the spectrum and mask all structural detail. The high-resolution NMR spectra obtained are then completely determined by the isotropic chemical shifts and the scalar part of the J coupling, and the individual linewidths are determined by the correlation time for molecular reorientation. Distance-dependent restraints are then established dynamically by their ''through space'' dipole-dipole interactions. Through a series of one-, two-, three-, or even higher-dimensional NMR experiments it is often possible to determine solution structures of soluble proteins [1–6]. Using these techniques one can even determine structures of small membrane peptides or protein fragments in detergent micelles [7–16].

Solid-state NMR techniques are generally designed to make use of the orientation-dependent interactions present in completely or partially ordered systems. These spectra are typically very broad and their complex line shapes are deter-

*Author to whom correspondence should be addressed.

mined by the highly anisotropic molecular reorientations typical of these systems. Structural information can easily be obtained from these tensor interactions. For example, the quadrupolar splitting for deuterium can be used to determine C-^{2}H bond orientation [17–20] and the anisotropic part of the chemical shift for ^{13}C and ^{15}N can be used to determine the orientation of chemical groups within a molecule [21–23]. Distances can be determined, at least in principle, from the dipole-dipole interaction between two nuclei. The ideal nucleus for this purpose would be ^{1}H because of its large magnetic moment and the resulting strong dipolar coupling. In partially ordered biological systems, however, the large abundance of ^{1}H usually results in ^{1}H NMR spectra which are so strongly broadened by multiple dipolar couplings that it is impossible to resolve inequivalent protons. Nonetheless, through isotopic labeling, it is possible to use the dipole-dipole coupling to determine both orientation and distance [24–27].

The range of dipolar couplings available is from 0 to about 118 kHz (for two ^{1}H nuclei separated by 1 Å). The strong distance dependence, going as $1/r^3$, limits the practical distance range, i.e., the linewidth of the spectrum ultimately sets a lower limit on the size of the dipolar coupling which can be measured. For example, for two ^{13}C nuclei separated by 5 Å, the dipolar coupling is at most about 60 Hz. When the linewidth of the ^{13}C spectrum is greater than this it becomes difficult to extract a reliable value for the dipolar coupling.

In powdered molecular solids, ^{13}C NMR line shapes are dominated by the heteronuclear dipolar coupling to abundant ^{1}H and by the anisotropic chemical shift of ^{13}C. High power ^{1}H decoupling can effectively eliminate this dipolar broadening [28,29], however the large anisotropic chemical shift (as large as 150 ppm, e.g., for carbonyl carbons) and the relatively short T_2's associated with fluctuations of such large couplings can make it difficult to extract ^{13}C-^{13}C dipolar couplings even as large 1 or 2 kHz from static powder pattern spectra. Single crystals would typically yield much sharper lines, however these are usually not available in sufficient size for biological materials. Fluid phase membrane powder samples yield ^{13}C spectra with linewidths from a few hundred Hz (for lipid methylene and methyl resonances) to 1 or 2 kHz for the lipid or peptide carbonyl groups. The rapid axially symmetric molecular reorientation about the bilayer normal reduces the chemical shift anisotropy as well as any ^{13}C-^{13}C dipolar couplings (depending on the orientation of the internuclear vector relative to the symmetry axis for the motion). The use of oriented membrane samples can reduce the linewidths to about 100 Hz, or even lower with the help of surfactants [30]. Finally, small vesicles, prepared by sonication, give high-resolution spectra because of the rapid isotropic tumbling of the vesicles. Unfortunately, this also removes the effects of any ^{13}C-^{13}C dipolar couplings.

By far the best resolution for membrane samples is obtained by magic angle spinning (MAS) combined with high power ^{1}H decoupling, in some cases giving linewidths of less than 0.1 ppm (less than 9 Hz at 90 MHz) for phospholipids in multilamellar dispersions. Of course, rotation of the sample at the magic angle removes not only the anisotropic chemical shift, but also the ^{13}C-^{13}C dipolar coupling. It is possible, however, to reintroduce dipolar couplings even while spinning at the magic angle [31–34]. There is now a rich variety of different methods for reintroducing either a homonuclear (such as between two ^{13}C nuclei) or a heteronuclear (such as between ^{13}C and ^{15}N nuclei) dipolar coupling between isolated pairs of nuclei. Samples are typically prepared by specific isotopic labeling at the two sites of interest and the dipolar coupling observed used to estimate the through space distance between the two labeled sites.

In a static or nonspinning polycrystalline powder sample with an anisotropic chemical shift, after the application of a single $\pi/2$ pulse, the resonance lines from individual crystallites, though initially in phase at $t=0$, dephase rapidly because the nuclei experience different chemical shifts depending on the orientation of the crystallite with respect to the magnetic field. In a MAS experiment, the second rank tensor interactions (such as the anisotropic part of the chemical shift) are projected onto the spinning axis. Thus, corresponding nuclei in all of the individual crystallites of the powder experience (over one rotor period) the same average chemical shift (the isotropic chemical shift) independent of the orientation of the crystallite. Then, the application of a single $\pi/2$ pulse to the nuclei of interest (assuming complete decoupling of abundant ^{1}H spins) will lead to a train of rotary echos, one occurring every rotation period [35]. Because of the anisotropic interactions, the resonances from any particular crystallite will shift in frequency, following distinct trajectories as the sample rotates. At the end of each rotor period, however, the resonances from all of the crystallites will again come into phase with one another since the average precession frequency over an integral number of rotor periods is always the isotropic chemical shift. In the case of two isolated spins coupled by an internuclear dipole-dipole interaction, both their anisotropic chemical shifts and their dipolar coupling are refocused in this fashion by the sample rotation, effectively eliminating these interactions.

REDOR (rotational echo double resonance) and related pulse sequences [36–38] use a train of rotor-synchronized π pulses applied to one of the nuclei to interfere with the rotational refocusing of the heteronuclear dipole-dipole interaction by MAS. This leads to incomplete refocusing of the signal from the second spin and to a reduction in the amplitude of the rotary echoes. This effect can be used to measure quantitatively the strength of the dipolar interaction between unlike nuclei [39–45].

Similar experiments can be performed with dipolar coupled pairs of like nuclei. For example, in a SEDRA (simple excitation for dephasing of rotational echo amplitudes) experiment [46] one interferes with the refocusing of the magnetization of the coupled spins using a train of rotor synchronized π pulses, and one compares the amplitudes of the rotational echoes with and without the dephasing pulses. DRAMA (dipolar recovery at the magic angle) [47–49] uses a pair of $\pi/2$ pulses during each rotor cycle to accomplish much the same thing. By switching the phase of a ''rotor synchronized spin-locking'' rf field applied to the observe nucleus by $\pi/2$, after 1/4 rotor period, then back again after 3/4 rotor periods, the MELODRAMA (melding of spin-locking and DRAMA) sequence reintroduces the homonuclear dipolar coupling but without the sensitivity to chemical shift of the DRAMA sequence [50].

Rotational resonance (R^2) reintroduces the dipolar coupling when the spinning rate, ν_R, or an integer multiple of it, $n\nu_R$, is set to match exactly the difference between the isotropic chemical shifts, $\delta\nu_i$, of the two dipolar coupled nuclei. The effect can be visualized crudely by considering the orientation of one of the spins as seen from the rotating frame of the other. Assume, for example, that at $t_0=0$ the two spins are parallel to each other and to the static magnetic field. At times greater than t_0 the second spin is seen by the first to precess at a frequency $\delta\nu_i$. At the same time, both spins are changing their orientation relative to H_0 since the sample is rotating about the magic angle. Exactly one rotor period later, τ_R, the first spin finds itself parallel to H_0 again, however the orientation of the second spin relative to H_0 and relative to the first spin depends on $\delta\nu_i$. If $\delta\nu_i$ is such that the second spin precesses by exactly 2π during τ_R, then at τ_R both spins are again parallel to H_0. Since at all integral multiples of τ_R the two spins have the same configuration relative to each other and to the magnetic field, there will be a cumulative effect from their dipolar coupling. On the other hand, if their relative orientations were uncorrelated, then there would be no effective dipolar coupling between them. This rotational resonance effect can lead to a dramatic broadening or even splitting of the resonances, depending on the strength of the dipolar coupling [51–53].

Each of these methods has its particular strengths and weaknesses. For example, SEDRA is sensitive to the rotational resonance condition since some dipolar dephasing may occur even in the absence of the dephasing pulse train. DRAMA works primarily with nuclei which have the same, or have very similar, isotropic chemical shifts. Rotational resonance is very sensitive to the sample spinning rate, and works best if the isotropic chemical shift difference is large. If the chemical shift difference is too large, and one cannot spin at $\nu_R=\delta\nu_i$, one can still use $n\nu_R=\delta\nu_i$, with $n=2,3,4,\ldots$. However, for $n>1$ the effect becomes quite sensitive to the values and orientations of the two different chemical shift tensors [52]. This sensitivity to the shift tensors and to the sample spinning rate can be either an advantage or a disadvantage, depending on the application. Peersen *et al.* [54] describe some of the critical technical requirements for rotational resonance, including the effect of ^{1}H decoupling power.

There have recently been a number of modifications to these basic techniques which have tried either to extend their applicability or minimize or eliminate some of their weaknesses. These include transferred echo double resonance (TEDOR) [37], which is aimed primarily at eliminating the background signal from *S* spins not coupled to *I* spins; CEDRA (controlled SEDRA) [55], which attempts to reduce the sensitivity of SEDRA to dipolar dephasing in the absence of the dephasing pulse train, as does *t*-SEDRA [56,57]. BDR (broadband dipolar recoupling) [58] and RFDR (radio frequency driven dipolar recoupling) [58,59] try to reduce the sensitivity of rotational resonance to the sample spinning rate by introducing a train of rotor synchronized π pulses to help enhance dipolar dephasing off-rotational resonance. The development of this field is advancing rapidly with a variety of new one- and two-dimensional experiments reported [53,58,60–66]. In the rest of this paper we will concentrate on the applications of rotational resonance to membrane and model membrane systems.

While most rotational resonance experiments to date have been performed on solid powders, there have been a number of applications to membrane systems. Peersen *et al.* [67] used rotational resonance to measure the distance between five different pairs of ^{13}C labeled carbonyl and methyl groups in a hydrophobic α-helical undecapeptide, either in crystalline powders or incorporated into 1,2-palmitoyl-*sn*-glycero-3-phosphocholine (DPPC) bilayers. For the bilayer samples the measurements were made at a temperature of -40 °C to eliminate effects of molecular reorientation. The distances measured ranged from 3.7 to 6.8 Å and the agreement between powder and bilayer measurements was quite good, showing that the α-helical crystal structure was maintained in the lipid environment, at least at -40 °C. Smith *et al.* [68] used doubly ^{13}C labeled DPPC to measure the distance between the *sn*-1 chain carbonyl and the 2-position methylene carbon of the *sn*-2 chain, finding a distance significantly shorter than in the crystal structure (4.5–5.0 Å compared to 5.3–5.5 Å for the crystal). This result was seen both at -50 and at $+5$ °C. Using mixtures of singly labeled lipids, either 1-palmitoyl,2-[2-^{13}C]palmitoyl PC or 1-palmitoyl, 2-[1-^{13}C]palmitoyl PC with DPPC doubly labeled either at the carbonyl (1-carbon) or at the first methylene carbon (2-carbon), they measured intermolecular dipolar couplings between lipids as well as between the lipids and the synthetic transmembrane segment of glycophorin-A which was ^{13}C labeled at [4-^{13}C]tyrosine-93.

In another publication, Smith *et al.* [69] used rotational resonance to measure distances between peptide backbone carbonyl and α carbons for four different doubly labeled synthetic glycophorin-A transmembrane segments incorporated into chain predeuterated 1,2-dimyristoyl-*sn*-glycero-3-phosphocholine (DMPC) bilayers. These were [1-^{13}C]val-80 to [2-^{13}C]gly-83, [1-^{13}C]met-81 to [2-^{13}C]gly-83, [1-^{13}C]ile-91 to [2-^{13}C]gly-94, and [1-^{13}C]ile-95 to [2-^{13}C]gly-98. The results of these measurements, which were performed at both -50 and $+5$ °C, are consistent with an α-helical structure near the center of the transmembrane segment but somewhat larger distances near the end of the segment suggest that the helix may unravel slightly near the membrane surface.

A follow-up study looked at dimer formation of the bilayer spanning glycophorin segments in deuterated DMPC. There, Smith and Bormann [70] used [^{13}C]-methyl labeled and [^{13}C]-carbonyl labeled peptides in a 1:5 molar ratio and measured rotational resonance magnetization exchange curves for the [^{13}C]-methyl label. This insures that the observed signal is predominantly due to (heterolabeled) dimers formed from one methyl labeled and one carbonyl labeled peptide. The strongest intermonomer dipolar coupling of the four preparations used was observed for the [$^{13}CH_3$]val-80/[^{13}C=O]gly-79 sample. The only other significant coupling observed was between [$^{13}CH_3$]val-84 and [^{13}C=O]gly-83. While these experiments could not precisely determine these internuclear distances, they did demonstrate that these four residues were located at the dimer interface and they established an upper limit of about 6 Å to the distance between them.

There has also been a series of experiments performed with bacteriorhodopsin, the light harvesting protein from *halobacterium halobium*. In the first paper of this series, Creuzet *et al.* [71] showed that it was possible to use rotational resonance to study the conformation at −30 °C of retinal, doubly ^{13}C labeled at the C-8 and C-18 carbons, incorporated into bacteriorhodopsin. Thompson *et al.* [72] then used bacteriorhodopsin with biosynthetically incorporated [ϵ-^{13}C]lysine-216 and synthetic [14-^{13}C] retinal to study the conformation of the retinal-protein Schiff base linkage in the stable states of dark-adapted bacteriorhodopsin at −50 °C. Lakshmi *et al.* [73] examined the *M* photointermediate state of the same system. To stabilize the photointermediate state, the preparation and experiments were performed at −60 °C. A series of experiments aimed at identifying and measuring the distance between [19-^{13}C]retinal and the nearest biosynthetically incorporated [4-^{13}C]tryptophan residue in bacteriorhodopsin has also been undertaken, again at low temperature (from −60 to −65 °C) [74]. McDermott *et al.* [75] compared the results of samples of bacteriorhodopsin containing doubly labeled retinal, either [8,18-$^{13}C_2$] retinal or [8,16(17)-$^{13}C_2$] retinal in samples presumably prepared as in the papers cited above and performed at similar temperatures, with studies of the similarly labeled model compound, polycrystalline retinoic acid. Here they demonstrated the utility of the sensitivity of higher-order rotational resonance (with $n>1$) on the relative orientations of the chemical shift and dipolar tensors for studying the relative orientations of the different chemical groups.

All of these studies were performed at low temperatures because molecular reorientation during the experimental time scale would result in a reduction in the dipolar couplings observed due to motional averaging. Without separate methods for measuring the nature and extent of motional averaging, it will not be possible to interpret the couplings observed directly in terms of a distance between the two labeled nuclei. Of course the physiological state of the membrane is the one of most direct interest and one can never be sure that measurements made at −60, or even at +5 °C in a gel phase lipid bilayer, will be the same as what would have been obtained under physiological conditions in a fluid membrane. To examine the effects of molecular reorientation on the measurement of dipolar couplings by rotational resonance and to determine the extent to which this technique can be used under more nearly physiological conditions, we have studied a simple model system composed of well characterized, synthetic, amphiphilic, bilayer-spanning peptides [17,19,76–82] both in polycrystalline powders and incorporated into fully hydrated DMPC bilayers. We have performed the model membrane experiments both at low temperatures and in the fluid or liquid crystalline bilayer phase. The following section describes the sample preparation, the NMR experimental procedures used, and the methods of data analysis and simulation. We then present the results of the experiments together with our estimates of uncertainties of the simulation parameters. Finally we discuss the implications for applications of such techniques to membrane systems in general.

MATERIALS AND METHODS

The lipid used in these experiments was 1-2-dimyristoyl-*sn*-glycero-3-phosphocholine (DMPC) obtained from Avanti Polar Lipids (Alabaster, Alabama). The two peptides used in the experiments both have the sequence

acetyl-lys-lys-gly-$(leu)_{16}$-lys-lys-ala-amide,

differing only in the position of the ^{13}C labels in the molecules, and were prepared by solid phase synthesis using procedures described by Davis *et al.* [17]. The positions of the labels are illustrated in Fig. 1. The first peptide, [1-^{13}C]leu_{11}:[α-^{13}C]leu_{12}, has the carbonyl of leu-11 and the α carbon of leu-12 labeled. The second peptide, [1-^{13}C]leu_8:[α-^{13}C]leu_{11}, has the carbonyl of leu-8 and the α carbon of leu-11 labeled. These two peptides are first studied in their polycrystalline form and then incorporated in a lipid bilayer using the protocol described below.

BILAYER MIXTURE

The lipid/peptide mixtures contained 8 mol % of peptide. First 40 mg of dry lipid powder and 13.3 mg of peptide were mixed together and dissolved in 5 ml of MeOH. The mixture was then rotovapped to remove the MeOH, leaving a film against the wall of the round bottom flask. Next the flask was placed under vacuum and pumped overnight using a cold trap to remove any excess solvent left in the sample. Finally the sample was removed from the flask and placed in a small culture tube and weighed. It was then rehydrated using a buffer solution of 20 mM potassium phosphate, pH 7.0. An amount of buffer equal to three quarters of the dry sample's weight was used. The hydrated sample was transferred into a rotor and gently packed using a centrifuge.

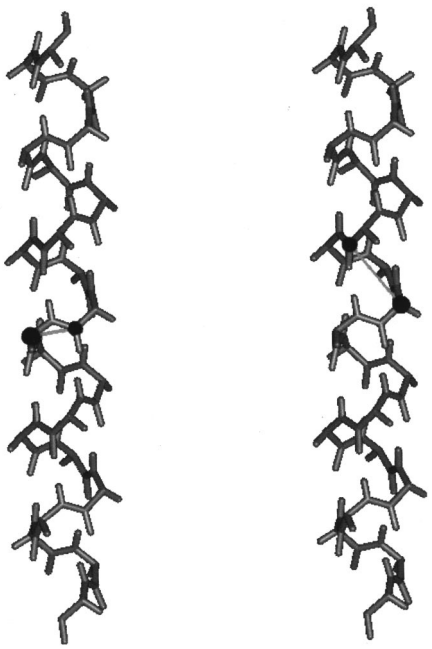

FIG. 1. The backbones of the two peptides showing, in black, the position of the ^{13}C labels. The peptide on the left is [1-^{13}C]leu_{11}:[α-^{13}C]leu_{12} and that on the right is [1-^{13}C]leu_8:[α-^{13}C]leu_{11}.

NMR

The experiments were all performed using a home built spectrometer operating at a ^{1}H frequency of 360 MHz (90.5 MHz for ^{13}C). The MAS probe is a home built double tuned probe using a standard Doty 5 mm high speed spinning assembly (Doty Scientific, Columbia, SC).

The pulse sequence used in the preliminary experiments was a single 90° pulse with proton decoupling during acquisition. The $^{13}C\pi/2$ pulse was 6 μs for all the experiments and the decoupling frequency was set to the leucine methyl proton resonance. The decoupling level corresponded to a $90°\pi/2$ proton pulse of 6.5 μs. By measuring the distance between the two isotropic lines obtained with the sample spinning at high speed, well off rotational resonance, we determined the spinning rate necessary to set the R^2 condition, $\nu_R = 10.897$ kHz. The spectrometer ^{13}C frequency was set so that ν_0 was at the center of the two lines to accommodate the pulse sequence described in the next section. Each spectrum was acquired using CYCLOPS [83] phase cycling which corrects for quadrature imperfections. The recycle delay time between sequence repetitions was about one minute for both the powder samples and the lipid/peptide mixtures. All of the experiments on both peptides were performed using the same conditions, the only variations being the number of points obtained for the exchange curves. The spectra for the solid powders were acquired at room temperature. In all cases, the spinning rate was maintained within ± 3 Hz. For the dry powders 400 scans were sufficient, while the lipid/peptide/buffer mixtures required 2000 scans since there was less labeled material in the rotor.

The sample temperature was controlled by regulating the temperature of a copper oven enclosing the spinning assembly and by adjusting the temperature of the air used for spinning the sample to have the same temperature at the outlet of the spinner. The lipid/peptide mixtures were studied at two different temperatures, -10 °C and 40 °C, corresponding to the gel and liquid crystalline phase of the lipid, respectively. The low temperature experiments were only performed at $n = 2$ since we were unable to spin reliably at 10.897 kHz at that temperature. At the higher temperature, we were able to obtain exchange curves for both $n = 1$ and 2.

Simulations were performed on an IBM R/6000 computer using software provided by Dr. Malcolm Levitt of the University of Stockholm in Sweden.

ROTATIONAL RESONANCE

A detailed description of rotational resonance (R^2) is given by Levitt *et al.* [52]. The sample, containing a dipolar coupled pair of like spin nuclei, is spun at a rate ν_r such that $n\nu_r$ is equal to $\Delta\nu^{iso}$, where $\Delta\nu^{iso}$ is the difference in frequency between the two lines due to their difference in isotropic chemical shift. n is a small integer, typically $n = 1$ or 2. At precise rotational resonance, the narrow lines broaden and split into two separate doublets. This broadening is due to the reintroduction of the dipolar coupling between the two spins and allows the measurement of the strength of this interaction which is proportional to $\langle 1/r_{IS}^3 \rangle$, where r_{IS} is the internuclear distance. The value of the dipolar coupling can be obtained in two ways. If the coupling is very strong, its value can be obtained by simulating the line shapes. On the other hand, if the dipolar coupling is weak and the two-spin dipolar broadening is of the order of the broadening due to other mechanisms, the value of the coupling is obtained through a magnetization exchange experiment, where the magnetization is made to oscillate from one site to the other. The rate of magnetization exchange is strongly enhanced by the rotational resonance condition. This oscillation is simulated numerically using the known chemical shift tensors and, by comparison with experiment, it is possible to obtain distance information. Depending on the value of n, the exchange curves can be sensitive to many parameters, namely the internuclear distance, the principal values of the chemical shielding tensors, their orientations, and the J coupling [52]. The importance of the CSA information grows with increasing value of n, but at $n = 1$, assuming that the difference in isotropic chemical shift is much greater than the CSA of either of the spins, the dependence on CSA orientation is minimal.

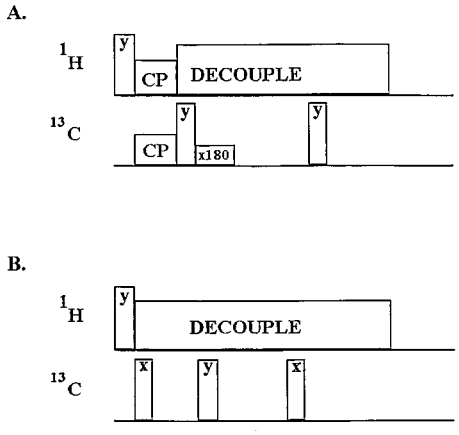

FIG. 2. Pulse sequences used in rotational resonance (R^2): (a) original sequence using cross polarization (CP); (b) sequence used in this work. The short, intense pulses indicated are 90° rotations about the axes indicated. In (a) the variable delay τ is between the selective 180° pulse and the nonselective 90° pulse. In (b), the delay between the ^{13}C x and y pulses is $\tau_1 = 1/2\Delta\nu_{iso}$, and the variable delay τ is between the nonselective y pulse and the final x pulse.

The original R^2 experiment was performed using the pulse sequence shown in Fig. 2(a) [51]. It begins with cross-polarization (CP) contact pulses, which are optional. A nonselective ''flip-back'' pulse then places the ^{13}C magnetization back along the z direction. This is followed by a ''soft'' 180° pulse to invert *one* of the two lines of interest. Finally, after a variable evolution time, another hard pulse is applied to return the magnetization to the x-y plane for data acquisition. There are three drawbacks to this approach. First, the use of a soft pulse to invert one line means tuning the spectrometer frequency on the line to be inverted, unless the spectrometer frequency can be switched. If the spectral width is very large it may not be possible to include the whole spectrum in the available window unless one uses a smaller dwell time which reduces the resolution of the spectrum. Replacing the soft pulse by a Dante sequence [84–86] can alleviate this problem. The second difficulty arises from the long soft pulse itself since the evolution of the spin system during this pulse is not explicitly accounted for in the simu-

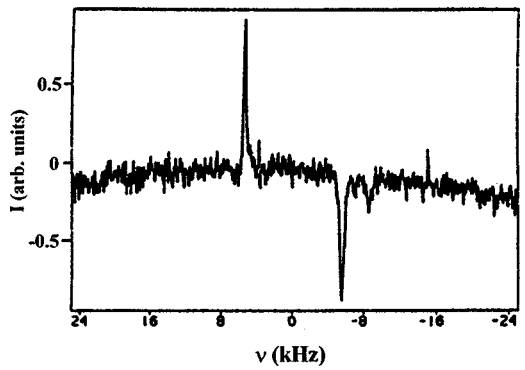

FIG. 3. Example of an ''exchange spectrum'' used in measuring the magnetization exchange curves. The spectrum shown is for the DMPC/[1-^{13}C]leu$_{11}$:[α-^{13}C]leu$_{12}$ sample at rotational resonance, $n=1$. Two hundred scans were accumulated for this spectrum.

lations. Third, a weak pulse has a length which is comparable to or even long compared to τ_R, the rotor period. Thus, if the CSA of the selected line is large, then during the weak pulse its effectiveness is variable since different spin packets move in and out of the pulse's bandwidth, resulting in incomplete inversion of many of the spins. Clearly, if one resonance has a large CSA and the other's is small, then when using a soft inversion pulse one should invert the line with the smaller CSA.

We have chosen to use a different pulse sequence, shown in Fig. 2(b), which minimizes these problems. A variation of this sequence is described by Geen *et al.* [87]. The spectrometer frequency is set exactly at the center between the two ^{13}C lines, and the first 90° pulse brings the magnetization into the *x-y* plane. The system then evolves for a time τ_1 equal to the time required for the magnetizations of the two spin species to become antiparallel. With ω_0 set half-way between them, this corresponds, at rotational resonance, to $\tau_1=\tau_R/2=1/2\Delta\nu^{\mathrm{iso}}$, where $\Delta\nu^{\mathrm{iso}}$ is the difference between the isotropic chemical shifts of the two nuclei of interest, and τ_R is the rotation period of the sample. The second pulse rotates these magnetization vectors back to the *z* axis, one parallel and one antiparallel to the *z* direction. The spins are then left to evolve for a variable period of time τ. One last pulse returns the vectors to the *x-y* plane where the signal can be acquired. Figure 3 shows a typical spectrum obtained using this sequence. Even this preparation sequence is imperfect since the physical rotation of the sample during τ_1 results in imperfect alignment of the two spin packets so that for some crystallite orientations the phase accumulated during τ_1 will not be exactly 90°.

RESULTS AND DISCUSSION

[1-^{13}C]leu$_{11}$:[α-^{13}C]leu$_{12}$ peptide in polycrystalline form

The exchange data at $n=1,2$ and off-rotational resonance for the dry peptide powder form of the [1-^{13}C]leu$_{11}$:[α-^{13}C]leu$_{12}$ peptide, which is ^{13}C labeled on adjacent leucine residues, are shown in Fig. 4(a). The squares and triangles represent the experimental data at $n=1$ (filled squares), $n=2$ (filled triangles), and off-rotational resonance (open squares) and the solid and dashed lines denote the best-fitting simulated curves. Not all of the simulation parameters necessary to fit the data (see Table II) are obtained directly from the R^2 experiment. As mentioned earlier, the orientation of each chemical shielding tensor relative to a given molecular reference frame must be known. In addition, the principal values of the CSA tensor, the *J* coupling, the decay time for the antiphase longitudinal polarization (or zero quantum relaxation time), T_{ZQ}, and finally $R_{\mathrm{IS}}=\langle 1/r_{\mathrm{IS}}^3\rangle^{-1/3}$, are all parameters of the simulation. A lower limit for the zero-quantum relaxation time, T_{ZQ}, can be estimated from the linewidth of the spectra off-rotational resonance using [72]

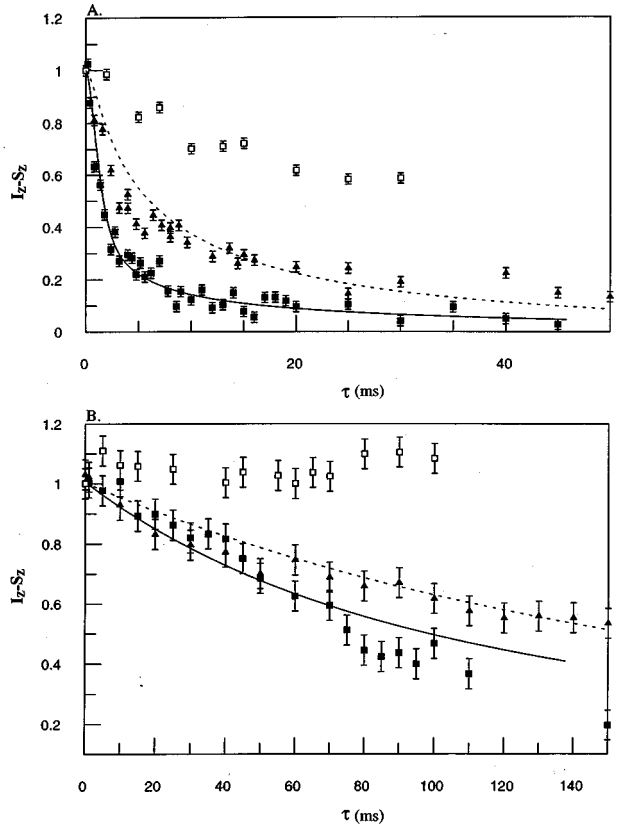

FIG. 4. Magnetization exchange data, $Iz-Sz$ vs τ, obtained for the peptides in the crystalline powder form. (a) Exchange at $n=1$ (closed squares), $n=2$ (closed triangles), and off-resonance (open squares) for the [1-^{13}C]leu$_{11}$:[α-^{13}C]leu$_{12}$ peptide. The simulated exchange curves (solid line for $n=1$ and dashed line for $n=2$) are obtained with a value of $R_{\mathrm{IS}}=2.1$ Å and $T_{\mathrm{ZQ}}=0.4$ ms. (b) Exchange at $n=1$ (closed squares), $n=2$ (closed triangles), and off-resonance (open squares) for the [1-^{13}C]leu$_8$:[α-^{13}C]leu$_{11}$ peptide. The simulated curves (solid line for $n=1$ and dashed line for $n=2$) are obtained with a distance of 4.6 Å and a value of $T_{\mathrm{ZQ}}=0.6$ ms. The error bars are estimated by determining the accuracy in measuring the area of the peaks in the spectrum. These error bars are directly related to the signal-to-noise ratio of the spectrum. The simulation parameters are given in Table II for the [1-^{13}C]leu$_{11}$:[α-^{13}C]leu$_{12}$ peptide and Table III for the [1-^{13}C]leu$_8$:[α-^{13}C]leu$_{11}$ peptide. Different scales are used for the data from the [1-^{13}C]leu$_{11}$:[α-^{13}C]leu$_{12}$ and [1-^{13}C]leu$_8$:[α-^{13}C]leu$_{11}$ to show the difference in the amplitude of the decay.

$$T_{\mathrm{ZQ}}=\frac{1}{\pi(\Delta_S+\Delta_I)},$$

where Δ_i is the full width at half height of each peak in the

TABLE I. Different values of η and δ for each label on the peptide.

Source	η	δ (ppm)	η_α	δ_α (ppm)
Naito *et al.*	0.84	71.0	0.44	19.67
Asakawa *et al.* [a]			0.77	16.42
Oas *et al.*	0.977	74.93		
Hinton [a]	0.97	91.7	0.3	10.64

[a]These values are obtained using theoretical calculation.

spectrum. However, the MAS spectrum does not give any information about the orientation of the principal axis of the CSA tensor. This is usually obtained from experiments done on single crystals of the molecule of interest or of a reasonable facsimile. Table I shows values of the CSA anisotropies δ_α and δ and of the asymmetry parameters, η_α and η, for the amino acid's α-carbon and carbonyl carbon chemical shielding tensors. δ and η are defined in terms of the elements of the chemical shift tensor by

$$\delta=\sigma_{33}-\frac{1}{3}\mathrm{tr}\overleftrightarrow{\sigma}, \quad \eta=\frac{\sigma_{22}-\sigma_{11}}{\delta}, \tag{1}$$

where σ_{33} is defined as the element furthest away from the isotropic position. Using a single crystal of *L* alanine, Naito *et al.* [88] measured all the parameters for both the carbonyl and the α carbon. From an *ab initio* chemical shift calculation, Asakawa *et al.* [89] determined both the orientation and the principal values of the CSA tensor for the α carbon of *L*-alanine residues. While Asakawa's value for the anisotropy was close to that measured by Naito *et al.* [88], the asymmetry parameter differs significantly. For the carbonyl, because of its larger anisotropy, the experimental CSA data for the carbonyl carbon are available from both Oas *et al.* [90] and Naito *et al.* [88]. These two sets of CSA values and the tensor orientation data are roughly consistent with each other and place the σ_{22} component along the C=O bond to within 10°. One difficulty with the use of these parameters in the present case is the fact that they were obtained for systems consisting of either a single or a pair of alanines, whereas we are working with a ''polyleucine'' system. The orientations and the principal values for the tensors will be slightly affected by the side chain differences since the electronic environment is slightly different.

In collaboration with Dr. J. Hinton (University of Arkansas, Fayetteville, AR), we performed *ab initio* calculations on a leu-leu model system with the geometry expected for adjacent leucines in an α helix. The results of this calculation are shown in the last row of Table I. The most noticeable difference between these and the results for alanine is in the anisotropy of the α carbon, which is of opposite sign. (Two ^{13}C spectra with anisotropies of opposite sign would look like mirror images of each other.) Unfortunately, no experimental data are available. The orientation of the principal axis of the carbonyl chemical shielding tensor, obtained by our calculation, shows the carbonyl σ_{22} direction almost along the C=O bond, in agreement with the results for alanine [88–90].

Obtaining a unique simulation of a curve with over 10 parameters is difficult due to the large number of possible sets of parameters which adequately fit the data. Levitt *et al.* [52], and others, have clearly shown that for an exchange curve taken on rotational resonance, i.e., at $n=1$, the only parameters which have a significant effect on the shape of the exchange curves are T_{ZQ} and R_{IS}. We have performed many series of simulations for $n=1$ and $n=2$ with varying parameters and have come to the same conclusion.

To determine the quality of a simulated curve, we calculated chi-squared (χ^2),

$$\chi^2=\sum\left\{\frac{1}{\sigma_i^2}[y_i-y(\tau_i)]^2\right\},$$

where y_i is an experimental point corresponding to the measured value of the difference magnetization at a given time τ_i and the σ_i are the uncertainties in each data point [91]. The $y(\tau_i)$ are the theoretical values determined using the simulation program.

Once the first two parameters T_{ZQ} and R_{IS} have been determined from the simulation at $n=1$, they can be further tested by attempting to fit the data at $n=2$. For $n>1$, the exchange curves are more sensitive to the other parameters described earlier, which are mainly related to the chemical shift tensors. Extensive simulation work was performed on the data to obtain a result with a minimum of ambiguity. To determine the range of possible values for each parameter, we performed a simple search in parameter space, first going through a series of values with large increments and then concentrating successively on the region of minimum χ^2. Figure 5(a) shows a surface map in parameter space describing the dependence of the quality of the fit, given by χ^2, on the distance R_{IS} and the value of the zero quantum relaxation time T_{ZQ}. The map shows a definite minimum for R_{IS} equal to 2.1 Å (corresponding to a dipolar coupling of 819 Hz) at $T_{ZQ}=0.4$ ms; the other parameters used are given in Table II. This value for R_{IS} is somewhat smaller than the value of 2.48 Å expected for an ideal α helix in the absence of motion. The value of $T_{ZQ}=0.4$ ms represents a lower limit obtained from the measurement of the linewidth of the two peaks on the spectra. Even though the map does not show a minimum in the T_{ZQ} direction, we cannot reduce T_{ZQ} any further in the simulations since this would imply that the spectral lines are wider than those observed (in reality the observed linewidth is probably slightly larger than $1/T_{ZQ}$). Figure 4(b) shows a one-dimensional cut of the surface map at $T_{ZQ}=0.4$ ms. A change in χ^2 of *unity* corresponds to a change in distance of 0.2 Å resulting in an uncertainty of ± 0.2 Å for our value of the distance, i.e., about $\pm 5\%$ or 10%. While this method of determining, and displaying, the uncertainty in R_{IS} may seem equivalent to the common method of showing several simulated exchange curves, it is more quantitative since the uncertainties in the raw data points are included in the analysis.

Surface maps were also calculated as functions of the asymmetry parameters, the anisotropies, and the relative orientations of the two CSA tensors (not shown). These maps were essentially flat, confirming the independence of the fit to these parameters. The second Euler angle, β, of the carbonyl carbon CSA tensor is the only parameter, other than R_{IS} and T_{ZQ}, that has any noticeable effect on the results at $n=1$. The dependence on β, although the greatest for all these parameters, can still be considered to be negligible.

TABLE II. Simulation parameters for Fig. 4(a).

$\Delta\nu_I$	5448 Hz
δ_I	8265 Hz
η_I	0.97
α_I	120.0°
β_I	−30.0°
γ_I	0.0°
$\Delta\nu_S$	−5448 Hz
δ_S	−963 Hz
η_S	0.3
α_S	0.0°
β_S	60.0°
γ_S	0.0°
b_{IZ}	819 Hz
J_{IS}	0.0 Hz
ν_R	10 897 Hz ($n=1$); 5448 Hz ($n=2$)
T_{ZQ}	0.0004s

TABLE III. Simulation parameters for Fig. 4(b).

$\Delta\nu_I$	5448 Hz
δ_I	8265 Hz
η_I	0.97
α_I	120.0°
β_I	−90.0°
γ_I	0.0°
$\Delta\nu_S$	−5448 Hz
δ_S	−963 Hz
η_S	0.3
α_S	30.0°
β_S	149.0°
γ_S	0.0°
b_{IZ}	78 Hz
J_{IS}	0.0 Hz
ν_R	10 897 Hz ($n=1$); 5448 Hz ($n=2$)
T_{ZQ}	0.0006 s

This observation is in agreement with the results obtained by Thompson *et al.* [72] where they also studied the relative influence of each parameter for the various values of *n*.

For the exchange curves at $n=2$, obtained using the parameters from Table II, the χ^2 surface map shows that while neither asymmetry parameter has much influence on the quality of the fit, the dependence on the asymmetry of the carbonyl is much more pronounced than for the α carbon. These fits favor the values determined by both Naito [88] and by our *ab initio* results (see Table I). Overall, we observed that the parameters for the α carbon have little or no effect on the shape of the simulated curves due to the small value of its chemical shift anisotropy. At $n=2$, the most critical parameters (besides T_{ZQ} and R_{IS}) are the two Euler angles α and β which determine the orientation of the carbonyl chemical shielding tensor relative to the internuclear vector. Since the previously reported values of the anisotropy for the carbonyl group also differed from each other, although to a lesser extent than for the α carbon, we performed a set of simulations to determine the influence of such differences on the exchange curves and found that χ^2 changes by unity when the carbonyl anisotropy is varied by about 2%.

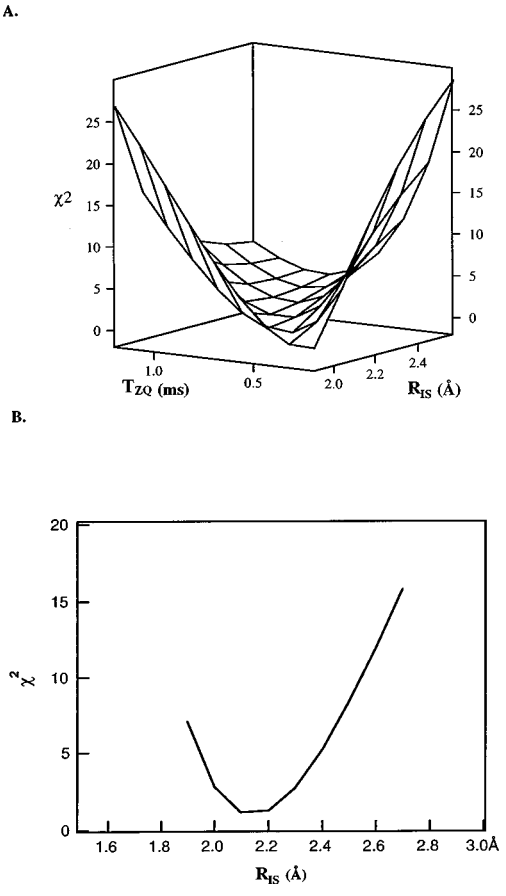

FIG. 5. (a) Two-dimensional surface map of χ^2 vs R_{IS} and T_{ZQ} for the [1-^{13}C]leu$_{11}$:[α-^{13}C]leu$_{12}$ peptide . (b) One-dimensional cut of the surface at $T_{ZQ}=0.6$ ms. A full set of simulation parameters used to obtain these maps is given in Table IV.

Figure 4(a) shows how the best curves fit the data for both $n=1$ and $n=2$. The analysis for $n=2$ revealed how the shape of the exchange curve is affected by changes in the parameters related to the two CSA tensors, and clearly illustrated the difficulties arising when attempting to obtain the distance parameter from curves obtained strictly at $n=2$, or at higher values of *n* where the interpretation is much more sensitive to the parameters characterizing the two CSA tensors.

[1-^{13}C]leu$_8$:[α-^{13}C]leu$_{11}$ peptide in polycrystalline form

Figure 4 also shows the data obtained from the exchange experiment on the second peptide in its crystalline powder form. Figure 4(b) gives the exchange curves at $n=1,2$, and off-rotational resonance. The CSA parameters used to simulate these curves are summarized in Table III. They are the same as for the [1-^{13}C]leu$_{11}$:[α-^{13}C]leu$_{12}$ peptide except for the Euler angles describing the orientation of the internuclear vector relative to the chemical shielding tensors, since the internuclear vector is different. With increased internuclear distance, the analysis becomes more challenging even though we now have reliable values for the anisotropies and the asymmetry parameters.

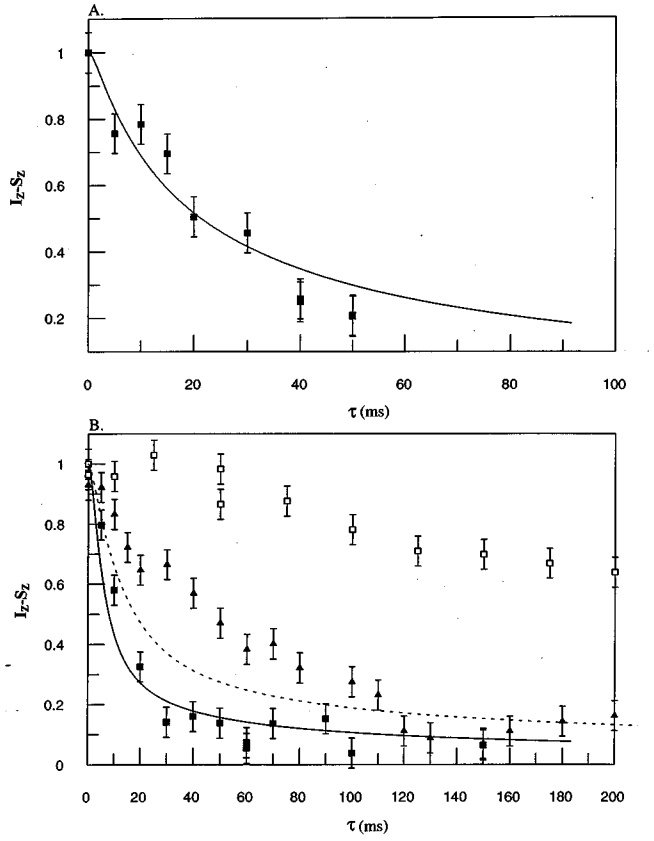

FIG. 6. Exchange curves, $Iz-Sz$ vs τ, for the DMPC/[1-^{13}C]leu$_{11}$:[α-^{13}C]leu$_{12}$ peptide mixture (a) at $-10°$; each point was obtained by measuring the area under the peaks of the spectrum. 500 repetitions were necessary to obtain a good signal-to-noise ratio. The repetition rate was 10 s. The solid line is the result of a simulation using parameters described in the text and in Table V. (b) At 40° with $n=1$ (closed squares), $n=2$ (closed triangles), and off-resonance (open squares). The simulation parameters for the curve (solid line for $n=1$ and dashed line for $n=2$) can be found in Table VI.

In order to determine the dipolar coupling in this case, we performed the same steps as previously for the [1-^{13}C]leu$_{11}$:[α-^{13}C]leu$_{12}$ peptide. As before, for $n=1$ the two parameters varied initially are T_{ZQ} and R_{IS} and a map of χ^2 is obtained (not shown). A value of $T_{ZQ}=0.6$ ms measured from the linewidth of the spectra of the peptide is used as a lower limit. The dipolar coupling of 78 Hz, obtained from the minimum on the map, corresponds to a distance of 4.6 ($\pm$0.3) Å. The average internuclear distance for the α-helical peptide from molecular-dynamics simulations [82] is 4.6 ($\pm$0.2) Å. In general, one can expect the internuclear distance to fluctuate by a certain amount. These fluctuations are expected to be more significant in the [1-^{13}C]leu$_8$:[α-^{13}C]leu$_{11}$ peptide than for the [1-^{13}C]leu$_{11}$:[α-^{13}C]leu$_{12}$ peptide because there are more flexible bonds between the two labeled positions. At high temperatures (52 °C), when the peptide is incorporated into a phospholipid bilayer, molecular-dynamics (MD) simulations show that the fluctuations in the internuclear distance between the labeled positions of the [1-^{13}C]leu$_8$:[α-^{13}C]leu$_{11}$ peptide are an order of magnitude greater than for the [1-^{13}C]leu$_{11}$:[α-^{13}C]leu$_{12}$ peptide, where the labels are placed on adjacent residues [81,82]. The MD simulation data for the [1-^{13}C]leu$_8$:[α-^{13}C]leu$_{11}$ peptide in a lipid bilayer show a $\pm$5% rms fluctuation in the internuclear distance. While such large fluctuations may not occur in the crystalline state, we can expect some fluctuations in the internuclear distance and, as a result, some decrease in the measured dipolar couplings.

TABLE IV. Simulation parameters for Fig. 6(a).

$\Delta\nu_I$	5448 Hz
δ_I	8265 Hz
η_I	0.97
α_I	120.0°
β_I	−30.0°
γ_I	0.0°
$\Delta\nu_S$	−5448 Hz
δ_S	−963 Hz
η_S	0.3
α_S	60.0°
β_S	0.0°
γ_S	0.0°
b_{IZ}	281 Hz
J_{IS}	0.0 Hz
ν_R	5448 Hz
T_{ZQ}	0.000 76 s

DMPC/[1-^{13}C]leu$_{11}$:[α-^{13}C]leu$_{12}$ peptide mixture

At low temperatures the lipid/peptide mixture is expected to be in a gel phase characterized by a high degree of lipid chain order and slow translational diffusion [76–78]. Figure 6(a) shows the exchange curve for this peptide/lipid mixture at −10 °C. The curve is obtained with the spinning rate set to match rotational resonance at $n=2$. Several attempts were made to obtain curves at $n=1$, but we were unable to spin reliably at that rate at −10 °C. The signal-to-noise ratio was also poorer for the experiments at lower temperature and the measured uncertainty in the peak areas was 6%. The value of T_{ZQ} was larger, however, having a value of about 0.87 ms compared to 0.4 ms in the solid. This narrowing of the NMR lines is likely the direct result of increased motion in the lipid bilayer compared to the solid. The simulation parameters are summarized in Table IV. The fit shown in Fig. 6(a) was obtained using a dipolar coupling of 281 Hz, which would suggest, in the absence of motional effects, an internuclear distance of 3.0 Å. Clearly the only consistent interpretation of this result is that motional averaging has reduced the dipolar coupling.

If the peptide diffused about its long axis, this motion would reduce the dipolar coupling by a factor $P_2(\cos\theta)$, where θ is the angle between the internuclear vector and the long axis of the peptide. For the [1-^{13}C]leu$_{11}$:[α-^{13}C]leu$_{12}$ peptide, this angle is 83° and this corresponds to a scaling factor of 0.48. This is sufficient to account for the observed reduction of the dipolar coupling, giving an internuclear distance of 2.35 Å, which is somewhat longer than the value deduced from the powder data, but agrees with the expected value (2.48 Å) within the error of the measurement.

In a ^{2}H NMR study of an amide-exchange labeled

TABLE V. Simulation parameters for Fig. 6(b).

$\Delta\nu_I$	5448 Hz
δ_I	578.6 Hz
η_I	0.0
α_I	0.0°
β_I	−90.0°
γ_I	0.0°
$\Delta\nu_S$	−5448 Hz
δ_S	298.6 Hz
η_S	0.0
α_S	0.0°
β_S	81.0°
γ_S	0.0°
b_{IZ}	211 Hz
ϕ_0	0.0°
θ_0	0.0°
J_{IS}	0.0 Hz
ν_R	10 897 Hz ($n=1$); 5448 Hz ($n=2$)
T_{ZQ}	0.0009 s

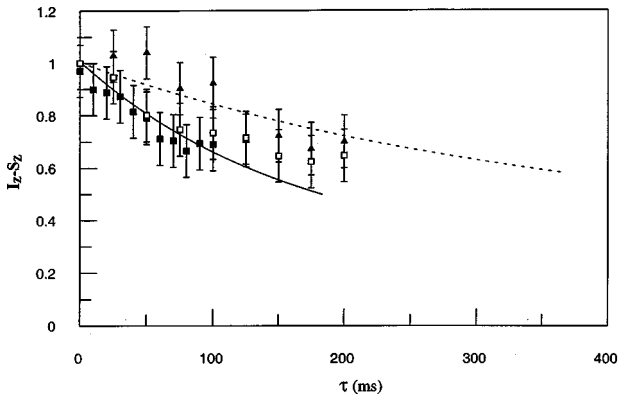

FIG. 7. Exchange curves, $Iz-Sz$ vs τ, obtained for the DMPC/[1-^{13}C]leu$_8$:[α-^{13}C]leu$_{11}$[1-^{13}C]leu$_8$:[α-^{13}C]leu$_{11}$ peptide mixture at 40° and at $n=1$ (closed squares), $n=2$ (closed triangles), and off-resonance (open squares). The symbols with the error bars represent the experimental data and the solid lines ($n=1$) and dashed line ($n=2$) denote the best fit. Each point is determined by measuring the area under the peaks in the spectrum. 500 repetitions were necessary to obtain sufficient signal to noise. The recovery period was set to 10 s. The fitting parameters are given in Table VI.

peptide/lipid system similar to ours, Pauls *et al.* [92] determined that in the gel phase the peptide spectra displayed an asymmetry parameter and a quadrupolar splitting characteristic of an immobile system. Based on the results from these ^{2}H NMR experiments, we conclude that at low temperatures the peptide is immobile on the time scale of the CSA interaction and that the CSA parameters are the same as for the solid powder, at least for the carbonyl label which has the larger anisotropy (approximately 8 kHz, Table II). In contrast, the dipolar coupling measured in the solid is only of the order of 500 Hz. It is possible that at −10°, the peptide axially diffuses at a rate sufficient to account for the reduction of the dipolar coupling and, perhaps, a reduction of the small α-carbon anisotropy (which has a value of approximately 1 kHz, Table II), and yet does not average the much larger chemical shift anisotropy of the carbonyl carbon (more comparable to the ^{2}H quadrupolar splitting [92]). The observed exchange data and the simulation are, therefore, consistent with intermediate rate axial diffusion of the peptide at −10° C. On the other hand, in the liquid crystalline phase, the ^{2}H spectrum was axially symmetric [92], implying that the peptide diffuses or reorients about its long axis at a rate greater than about 10^5-10^6 s^{-1} in that phase.

Figure 6(b) shows the exchange curves obtained for the DMPC/[1-^{13}C]leu$_{11}$:[α-^{13}C]leu$_{12}$ peptide sample at 40 °C. Comparing the $n=1$ data to the data obtained off-rotational resonance, we see a distinctly more rapid decay of the difference magnetization at rotational resonance even though the sample is in the fluid phase at 40°. At this temperature the lower limit of T_{ZQ} was determined to be 0.9 ms since the lines were even narrower due to the increased motional averaging in the fluid phase. Under these conditions we can no longer assume that the peptide is immobile even on the time scale of the chemical shift anisotropies. ^{2}H NMR shows that the peptide undergoes rapid axially symmetric reorientation in the liquid crystalline phase. Since the time scale of the ^{13}C CSA interaction is even longer than that of the ^{2}H quadrupolar interaction, the chemical shielding interaction is also averaged by this motion. This reduces the asymmetry parameter for both labeled positions to zero and the chemical shift anisotropies are reduced by the factor $\frac{1}{2}\{[3\cos^2(\beta_{PN})-1]+\eta\sin^2\beta_{PN}\cos 2\alpha_{PN}\}$, where (α_{PN},β_{PN}) are the Euler angles defining the orientations of CSA tensors relative to the diffusion axis. At 40 °C we have data at $n=1$, so the initial simulation is easier since we only have to determine the values of T_{ZQ} and R_{IS}. The parameters are summarized in Table V and the calculated curves are compared to the data in Fig. 6(b). The best fit corresponds to a motionally averaged dipolar coupling of 211.2 Hz which, if scaled by a factor 0.48, as for the low temperature case, would yield an estimated distance of 2.6 (±0.2) Å.

The scaling of the dipolar coupling by axial diffusion is nearly sufficient to explain the difference between the decay curves obtained for the polycrystalline powder and for the fluid phase membrane. Other motions, such as a wobbling of the molecule, would increase the averaging of the dipolar coupling, reducing the observed value and therefore leading to the measurement of an even smaller dipolar coupling. For example, in a study of the gramicidin D dimer in a membrane in the liquid crystalline phase, Prosser *et al.* [93] and Prosser and Davis [20] describe the dynamics of the peptide using two motions, the axial diffusion described earlier and a second wobbling motion with a longer correlation time. This second motion is still fast on the dipolar interaction time scale and could be considered as another averaging process. Molecular-dynamics simulations of our synthetic peptide [81,82] have shown that the peptide axis is tilted with respect to the bilayer normal with a mean relative orientation of about 15°, with rms fluctuations of about 5°, in agreement with previous x-ray diffraction measurements [79] and the ^{2}H NMR studies of gramicidin D [20,93]. The further reduction in the dipolar coupling for the [1-^{13}C]leu$_{11}$:[α-^{13}C]leu$_{12}$ peptide by a factor of 0.84 due to this wobbling of the diffusion axis relative to the bilayer normal results in an estimated internuclear distance of 2.44 Å.

TABLE VI. Simulation parameters for Fig. 7.

$\Delta\nu_I$	5448 Hz
δ_I	−4132 Hz
η_I	0.0
α_I	0.0°
β_I	90.0°
γ_I	0.0°
$\Delta\nu_S$	−5448 Hz
δ_S	481 Hz
η_S	0.0
α_S	0.0°
β_S	90.0°
γ_S	0.0°
b_{IZ}	34 Hz
J_{IS}	0.0 Hz
ν_R	10 897 Hz ($n=1$); 5448.55 Hz ($n=2$)
T_{ZQ}	0.00152 s

DMPC/[1-^{13}C]leu$_8$:[α-^{13}C]leu$_{11}$ peptide mixture

Figure 7 shows the exchange curves obtained for the DMPC/[1-^{13}C]leu$_8$:[α-^{13}C]leu$_{11}$ peptide sample at 40 °C, taken at $n=1$, $n=2$, and off-rotational resonance. These curves all lie within each other's experimental error. The best we can do here is to estimate an upper limit for the value of the motionally averaged dipolar coupling for this system, using the parameters obtained with the DMPC/[1-^{13}C]leu$_{11}$:[α-^{13}C]leu$_{12}$ peptide sample and from the [1-^{13}C]leu$_8$:[α-^{13}C]leu$_{11}$ peptide crystalline powder as a starting point. With a value for T_{ZQ} of 1.5 ms from the peak linewidths, we obtained the solid curves shown in Fig. 7 and a maximum value for the dipolar coupling of 34 Hz. This corresponds closely to the value obtained simply by scaling the powder value by a factor of 0.48×0.84. A coupling larger than this would lead to a noticeable difference between on- and off-rotational resonance exchange curves. This result clearly demonstrates the limitation of the technique for measuring dipolar couplings in the presence of motion (see Table VI).

CONCLUSION

The results of our study of these two peptides clearly show both the potential and the limitations of R^2. In the polycrystalline powders we were able to measure the internuclear dipolar couplings, and thereby deduce the internuclear distances, quite accurately for both peptides. The distances obtained, 2.1 ± 0.2 Å for the [1-^{13}C]leu$_{11}$:[α-^{13}C]leu$_{12}$ peptide and 4.5 ± 0.3 Å for the [1-^{13}C]leu$_8$:[α-^{13}C]leu$_{11}$ peptide, are close to the values expected for the equilibrated ideal α helix (2.48 and 4.6 Å). In the presence of axial diffusion of the peptide about its long axis, we can easily measure the dipolar coupling for the [1-^{13}C]leu$_{11}$:[α-^{13}C]leu$_{12}$ peptide, but the coupling for the [1-^{13}C]leu$_8$:[α-^{13}C]leu$_{11}$ peptide is too small to give a reliable value and we can only establish an upper limit to the coupling. To interpret the coupling observed for the [1-^{13}C]leu$_{11}$:[α-^{13}C]leu$_{12}$ peptide in the fluid phase in terms of an internuclear distance, we need precise information on the nature and time scales of the peptide motions. Rapid axial diffusion and the reorientation of this axis relative to the bilayer normal both act to reduce the observed dipolar coupling. Internal motions of the peptide, such as instability of the helical structure and local librational motions would also lead to some reduction in the observed dipolar coupling.

While the presence of motion limits the applicability of techniques for measuring internuclear distances through the internuclear dipolar coupling, a knowledge of the dynamics of the system should still permit the interpretation of these couplings in terms of average distances provided that the couplings are readily measurable. To measure weaker couplings, such as are found in the membrane fluid phase, it will be necessary to use higher power decoupling [54] and to search for systems with larger values of T_{ZQ} or to use nuclei with larger magnetic dipole moments than ^{13}C (e.g., ^{19}F).

ACKNOWLEDGMENTS

We would like to express our gratitude to Dr. J. Hinton for his help with the calculations of the chemical shift tensors for leucine, and to Dr. M. Levitt for his simulation program and his help in performing the simulations. Thanks are also due to William Gillespie for his suggestion for improving the regulation of our airflow system. We would also like to acknowledge the Natural Sciences and Engineering Research Council of Canada for financial support. D.B.L. would like to thank the program Fonds pour la Formation de Chercheurs et l'Aide à la Recherche (FCAR) of the province of Québec for financial support.

[1] R. R. Ernst, G. Bodenhausen, and A. Wokaun, *Principles of Nuclear Magnetic Resonance in One and Two Dimensions* (Oxford University Press, Oxford, 1987).
[2] G. M. Clore and A. M. Gronenborn, Protein Sci. **3**, 372 (1994).
[3] L. E. Kay, Prog. Biophys. Mol. Biol. **63**, 277 (1995).
[4] L. E. Kay, Cell Biol. **75**, 1 (1997).
[5] L. E. Kay, G. M. Clore, A. Bax, and A. M. Gronenborn, Nature (London) **249**, 411 (1990).
[6] H. Oschkinat, C. Griesinger, P. J. Kraulis, O. W. Sorensen, R. R. Ernst, A. M. Gronenborn, and G. M. Clore, Science **332**, 374 (1988).
[7] A. S. Arseniev, I. L. Barsukov, V. F. Bystrov, A. L. Lomize, and Yu. A. Ovchinnikov, FEBS Lett. **186**, 168 (1985).
[8] K.-J. Shon, Y. Kim, L. Colnago, and S. J. Opella, Science **252**, 1303 (1991).
[9] V. Yu. Orekov, G. V. Abdulaeva, L. Yu. Musina, and A. S. Arseniev, Eur. J. Biochem. **210**, 223 (1992).
[10] V. Yu. Orekov, K. V. Pervushin, and A. S. Arseniev, Eur. J. Biochem. **219**, 887 (1994).
[11] P. A. McDonnel, K. Shon, Y. Kim, and S. J. Opella, J. Mol. Biol. **233**, 447 (1993).
[12] G. D. Henry and B. D. Sykes, Methods Enzymol. **239C**, 515 (1994).
[13] S. J. Opella, Y. Kim, and P. A. McDonnel, Methods Enzymol. **239C**, 536 (1994).
[14] K. V. Pervushin, V. Yu. Orekhov, A. I. Popov, L. Yu. Musina,

and A. S. Arseniev, Eur. J. Biochem. **219**, 571 (1994).
[15] K. Mackenzie, J. H. Prestegard, and D. M. Engelman, J. Biomol. NMR **7**, 256 (1996).
[16] K. Mackenzie, J. H. Prestegard, and D. M. Engelman, Science **276**, 131 (1997).
[17] J. H. Davis, Biochim. Biophys. Acta **737**, 117 (1983).
[18] J. H. Davis, in *Isotopes in the Physical and Biomedical Sciences*, edited by E. Buncel and J. R. Jones (Elsevier, Amsterdam, 1991), Vol. 2.
[19] R. S. Prosser, J. H. Davis, F. W. Dahlquist, and M. A. Lindorfer, Biochemistry **30**, 4687 (1991).
[20] R. S. Prosser and J. H. Davis, Biophys. J. **66**, 1429 (1994).
[21] R. R. Ketchem, W. Hu, and T. A. Cross, Science **261**, 1457 (1993).
[22] Q. Teng, and T. A. Cross, J. Magn. Reson. **85**, 439 (1989).
[23] S. J. Opella, P. L. Stewart, and K. G. Valentine, Q. Rev. Biophys. **19**, 7 (1987).
[24] F. M. Marassi, A. Ramamoorthy, and S. J. Opella, Proc. Natl. Acad. Sci. USA **94**, 8551 (1997).
[25] Q. Teng, L. K. Nicholson, and T. A. Cross, J. Mol. Biol. **218**, 607 (1991).
[26] S. J. Opella, J. Gesell, and B. Bechinger, in *The Amphipathic Helix*, edited by R. M. Epand (CRC Press, Boca Raton, FL, 1994).
[27] C. H. Wu, A. Ramamoorthy, L. M. Gierasch, and S. J. Opella, J. Am. Chem. Soc. **117**, 6148 (1995).
[28] P. Tekely, P. Palmas, and D. Canet, J. Magn. Reson. **107**, 129 (1994).
[29] A. E. Bennett, C. M. Rienstra, M. Auger, K. V. Lakshmi, and R. G. Griffin, J. Chem. Phys. **103**, 6951 (1996).
[30] C. R. Sanders, Biophys. J. **64**, 171 (1993).
[31] J. M. Griffiths and R. G. Griffin, Anal. Chim. Acta **283**, 1081 (1993).
[32] J. Garbow and T. Gullion, *Carbon-13 NMR Spectroscopy of Biological Systems* (Academic Press, San Diego, 1995).
[33] S. O. Smith, K. Aschheim, and M. Groesbeek, Q. Rev. Biophys. **29**, 395 (1996).
[34] L. M. McDowell and J. Schaefer, Curr. Opin. Struct. Biol. **6**, 624 (1996).
[35] M.M. Maricq and J.S. Waugh, J. Chem. Phys. **70**, 3300 (1979).
[36] T. Gullion and J. Schaefer, Adv. Magn. Reson. **13**, 58 (1989).
[37] A. W. Hing, S. Vega, and J. Schaefer, J. Magn. Reson., Ser. A **103**, 151 (1993).
[38] A. W. Hing and J. Schaefer, Biochemistry **32**, 7593 (1993).
[39] S. M. Holl, G. R. Marshall, D. D. Beusen, K. Kociolek, A. S. Redlinski, M. T. Leplawy, R. A. McKay, S. Vega, and J. Schaefer, J. Am. Chem. Soc. **114**, 4830 (1994).
[40] A. W. Hing, N. Tjandra, P. F. Cottam, J. Schaefer, and C. Ho, Biochemistry **33**, 8651 (1994).
[41] T. Gullion, J. Magn. Reson., Ser. A **117**, 326 (1995).
[42] T. Gullion, Chem. Phys. Lett. **246**, 325 (1995).
[43] D. D. Mueller, A. Schmidt, K. L. Pappan, R. A. McKay, and J. Schaefer, Biochemistry **34**, 5597 (1995).
[44] K. T. Mueller, T. P. Jarvie, D. J. Aurentz, and B. W. Roberts, Chem. Phys. Lett. **242**, 535 (1995).
[45] T. P. Jarvie, G. T. Went, and K. T. Mueller, J. Am. Chem. Soc. **118**, 5330 (1996).
[46] T. Gullion and S. Vega, Chem. Phys. Lett. **194**, 423 (1993).
[47] R. Tycko, and G. Dabbagh, Chem. Phys. Lett. **173**, 461 (1990).
[48] R. Tycko and G. Dabbagh, J. Am. Chem. Soc. **113**, 9444 (1991).
[49] R. Tycko and S. O. Smith, J. Chem. Phys. **98**, 932 (1993).
[50] B.-Q. Sun, P. R. Costa, D. Kocisko, P. T. Lansbury, Jr., and R. G. Griffin, J. Chem. Phys. **102**, 702 (1995).
[51] D. P. Raleigh, M. H. Levitt, and R. G. Griffin, Chem. Phys. Lett. **146**, 71 (1988).
[52] M. H. Levitt, D. P. Raleigh, F. Creuzet, and R. G. Griffin, J. Chem. Phys. **92**, 6347 (1990).
[53] R. G. S. Spencer, K. W. Fishbein, M. H. Levitt, and R. G. Griffin, J. Chem. Phys. **100**, 5533 (1994).
[54] O. B. Peersen, M. Groesbeek, S. Aimoto, and S. O. Smith, J. Am. Chem. Soc. **117**, 7228 (1995).
[55] W. Zhu, C. A. Klug, and J. Schaefer, J. Magn. Reson., Ser. A **108**, 121 (1994).
[56] O. Weintraub, S. Vega, Ch. Hoelger, and H. H. Limbach, J. Magn. Reson., Ser. A **109**, 14 (1994).
[57] O. Weintraub, S. Vega, Ch. Hoelger, and H. H. Limbach, J. Magn. Reson., Ser. A **110**, 12 (1994).
[58] D. K. Sodickson, M. H. Levitt, S. Vega, and R. G. Griffin, J. Chem. Phys. **98**, 6742 (1993).
[59] A. E. Bennett, J. H. Ok, and R. G. Griffin, J. Chem. Phys. **96**, 8624 (1992).
[60] J. H. Ok, R. G. S. Spencer, A. E. Bennett, and R. G. Griffin, Chem. Phys. Lett. **197**, 389 (1992).
[61] T. Fujiwara, A. Ramamoorthy, K. Nagayama, K. Hioka, and T. Fujito, Chem. Phys. Lett. **212**, 81 (1993).
[62] N. C. Nielsen, H. Bildsoe, H. J. Jakobsen, and M. H. Levitt, J. Chem. Phys. **101**, 1805 (1994).
[63] J. M. Joers, R. Rosanske, T. Gullion, and J. R. Garbow, J. Magn. Reson., Ser. A **106**, 123 (1994).
[64] D. M. Gregory, D. J. Mitchell, J. A. Stringer, S. Kiihne, J. C. Shiels, J. Callahan, M. A. Mehta, and G. P. Drobny, Chem. Phys. Lett. **246**, 654 (1995).
[65] Y. K. Lee, N. D. Kurur, M. Helmle, O. G. Johannessen, N. C. Nielsen, and M. H. Levitt, Chem. Phys. Lett. **242**, 304 (1995).
[66] K. Takegoshi, K. Nomura, and T. Terao, Chem. Phys. Lett. **232**, 424 (1995).
[67] O. B. Peersen, S. Yoshimura, H. Hojo, S. Aimoto, and S. O. Smith, J. Am. Chem. Soc. **114**, 4332 (1992).
[68] S. O. Smith, J. Hamilton, A. Salmon, and B. J. Bormann, Biochemistry **33**, 6327 (1994).
[69] S. O. Smith, R. Jonas, M. Braiman, and B. J. Bormann, Biochemistry **33**, 6334 (1994).
[70] S. O. Smith and B. J. Bormann, Proc. Natl. Acad. Sci. USA **92**, 488 (1995).
[71] F. Creuzet, A. McDermott, R. Gebhard, K. van der Hoef, M. B. Spijker-Assink, J. Herzfeld, J. Lugtenburg, M. H. Levitt, and R. G. Griffin, Science **251**, 783 (1991).
[72] L. K. Thompson, A. E. McDermott, J. Raap, van der C. M. Wielen, J. Lugtenburg, J. Herzfeld, and R. G. Griffin, Biochemistry **31**, 7931 (1992).
[73] K. V. Lakshmi, M. Auger, J. Raap, J. Lugtenberg, R. G. Griffin, and J. Herzfeld, J. Am. Chem. Soc. **115**, 8515 (1993).
[74] M. Auger, K. V. Lakshmi, E. M. M. de Brabander–van den Berg, S. J. Rosselt, T. Marti, H. G. Khorana, S. K. Das Gupta, W. B. S. van Liemt, J. Raap, J. Lugtenberg, R. G. Griffin, and J. Herzfeld (private communication).
[75] A. E. McDermott, F. Creuzet, R. Gebhard, K. van der Hoef,

M. H. Levitt, J. Herzfeld, J. Lugtenburg, and R. G. Griffin, Biochemistry **33**, 6129 (1994).
[76] J. H. Davis, D. M. Clare, R. S. Hodges, and M. Bloom, Biochemistry **22**, 5298 (1983).
[77] J. C. Huschilt, R. S. Hodges, and J. H. Davis, Biochemistry **24**, 1377 (1985).
[78] M. R. Morrow, J. C. Huschilt, and J. H. Davis, Biochemistry **24**, 5396 (1985).
[79] J. C. Huschilt, B. M. Millman, and J. H. Davis, Biochim. Biophys. Acta **979**, 139 (1989).
[80] J. H. Davis, M. Auger, and R. S. Hodges, Biophys. J. **69**, 1917 (1995).
[81] K. Belohorcova, M.Sc. thesis, University of Guelph, Guelph, Ontario, Canada (1995).
[82] K. Belohorcova, J. H. Davis, T. B. Woolf, and B. Roux, Biophys. J. **73**, 3039 (1997).
[83] D. I. Hoult and R. E. Richard, Proc. R. Soc. London, Ser. A **344**, 311 (1975).
[84] G. A. Morris and R. Freeman, J. Magn. Reson. **29**, 433 (1978).
[85] P. Caravatti, G. Bodenhausen, R. R. Ernst, J. Magn. Reson. **55**, 88 (1983).
[86] J. M. Griffiths, T. T. Ashburn, M. Auger, P. R. Costa, R. G. Griffin, and P. T. Lansbury, Jr., J. Am. Chem. Soc. **117**, 3539 (1995).
[87] H. Geen, M. H. Levitt, and G. Bodenhausen, Chem. Phys. Lett. **200**, 350 (1992).
[88] A. Naito, S. Ganapathy, K. Akasaka, and C. A. McDowell, J. Chem. Phys. **74**, 3190 (1981).
[89] N. Asakawa, H. Kurosu, I. Ando, A. Shoji, and T. Ozaki, J. Mol. Struct. **317**, 119 (1994).
[90] T. G. Oas, C. J. Hartzell, T. J. McMahon, G. P. Drobny, and F. W. Dahlquist, J. Am. Chem. Soc. **109**, 5956 (1987).
[91] P. R. Bevington, *Data Reduction and Error Analysis for the Physical Science* (McGraw-Hill, Toronto, 1969).
[92] K. P. Pauls, A. L. MacKay, O. Söderman, M. Bloom, A. K. Tanjea, and R. S. Hodges, Eur. Biophys. J. **12**, 1 (1985).
[93] R. S. Prosser, S. I. Daleman, and J. H. Davis, Biophys. J. **66**, 1415 (1994).